Biopolymer Electrospun Nanofibers

M.MOHAMMADIAN[1], A.K.HAGHI[2]*

[1] Islamic Azad University, Department of Textile Engineering, Kashan Branch, Kashan, Iran

[2] University of Guilan, P.O.Box 3756, Rasht, Iran

Silk fibroin, from Bombyx mori solutions were electrospun into nanofibers with circular and ribbon like morphology. Diameters of the electrospun fibers were ranged from 60 to 7000 nm. The effects of electrospinning temperature, solution concentration and electric field on the formation of nanofibers and their morphology were studied. Optical and scanning electron microscope were used to study the morphology and diameter of electrospun nanofibers. It was observed that the nanofibers morphology depends on the electrospinning parameters and became flattened with ribbon like shape with increasing the electrospinning temperature. The nanofiber diameter increased with the increase in the concentration of silk solution at all electrospinning temperature. Electric field showed different effects on the nanofiber morphology at 25°C. Referring to the literature the probable mechanism responsible for the change of morphology was pointed out. Response surface methodology (RSM) was used to obtain a quantitative relationship between selected electrospinning parameters and average fiber diameter and its distribution. It was shown that concentration of silk fibroin solution and electrospinning temperature had a significant effect on the fiber diameter.

Keywords: biopolymers, scanning electron microscope, morphology, proteins, nanofibers, statistical analysis

In recent years, the electrospinning process has gained much attention because it is an effective method to manufacture ultrafine fibers or fibrous structures of many polymers with diameter in the range from several micrometers down to tens of nanometers [1]. In the electrospinning process, a high voltage is used to create an electrically charged jet of a polymer solution or a molten polymer. This jet is collected on a target as a non-woven fabric. The jet typically develops a bending instability and then solidifies to form fibers, which measures in the range of nanometers to 1 mm. Because these nanofibers have some useful properties such as high specific surface area and high porosity, they can be used as filters, wound dressings, tissue engineering scaffolds, etc.

Recently, the protein-based materials have been interested in biomedical and biotechnological fields. The silk polymer, a representative fibrous protein, has been investigated as one of promising resources of bio-technology and biomedical materials due to its unique properties [2]. Furthermore, high molecular weight synthetic polypeptides of precisely controlled amino acid composition and sequence have been fabricated using the recombinant tools of molecular biology. These genetic engineered polypeptides have attracted the researcher's attention as a new functional material for biotechnological applications including cellular adhesion promoters, biosensors, and suture materials.

Silks are generally defined as fibrous proteins that are spun into fibers by some Lepidoptera larvae such as silkworms, spiders, scorpions, mites and flies. Silkworm silk has been used as a luxury textile material since 3000 B.C., but it was not until recently that the scientific community realized the tremendous potential of silk as a structural material. While stiff and strong fibers (such as carbon, aramid, glass, etc.) are routinely manufactured nowadays, silk fibers offer a unique combination of strength and ductility which is unrivalled by any other natural or man-made fibers. Silk has excellent properties such as lightweight (1.3 g/cm^3) and high tensile strength (up to 4.8 GPa as the strongest fiber known in nature). Silk is thermally stable up to 250°C, allowing processing over a wide range of temperatures[3].The origins of this behaviour are to be found in the organization of the silks at the molecular and supramolecular levels, which are able to impart a large load bearing capability together with a damage tolerant response. The analysis of the fracture micro mechanisms in silk may shed light on the relationship between its microstructure and the mechanical properties. The anti-parallel β plated structure of silk gives rise to its structural properties of combined strength and toughness [3].

B. mori silk consists of two types of proteins, fibroin and sericin. Fibroin is the protein that forms the filaments of silkworm silk [3]. Fibroin filaments made up of bundles of nanofibrils with a bundle diameter of around 100 nm. The nanofibrils are oriented parallel to the axis of the fiber, and are thought to interact strongly with each other [3]. Fibroin contains 46% Glycine, 29% Alanine and 12% Serine. Fibroin is a giant molecule (4700 amino acids) comprising a "crystalline" portion of about two-thirds and an ''amorphous'' region of about one-third. The crystalline portion comprises about 50 repeats of polypeptide of 59 amino acids whose sequence is known: Gly-Ala-Gly-Ala-Gly-Scr-Gly-Ala-Ala-Gly- (Scr-Gly-Ala-Gly-Ala-Gly)s-Tyr. This repeated unit forms, β - sheet and is responsible for the mechanical properties of the fiber [1].

Silk fibroin (SF) can be prepared in various forms such as gels, powders, fibers, and membranes [9].Number of researchers has investigated silk-based nanofibers as one of the candidate materials for biomedical applications, because it has several distinctive biological properties including good biocompatibility, good oxygen and water vapour permeability, biodegradability, and minimal inflammatory reaction. Several researchers have also studied processing parameters and morphology of electrospun silk nanofibers using Hexafluoroacetone, Hexafluoro-2-propanol and formic acid as solvents. In all these reports nanofibers with circular cross sections have been observed.

* *email: Haghi@Guilan.ac.ir*

In the present paper, effects of electrospinning parameters are studied and nanofibers dimensions and morphology are reported. Morphology of fibers diameter of silk precursor were investigated varying concentration, temperature and applied voltage and observation of ribbon like silk nanofibers were reported. Furthermore, a more systematic understanding of the process conditions was studied and a quantitative basis for the relationships between average fiber diameter and electrospinning parameters was established using response surface methodology (RSM), which will provide some basis for the preparation of silk nanofibers with desired properties (Appendix).

Experiment part

Preparation of regenerated SF solution

Raw silk fibers (B.mori cocoons were obtained from domestic producer, Abrisham Guilan Co., IRAN) were degummed with 2 gr/L Na_2CO_3 solution and 10 gr/L anionic detergent at 100 ° C for 1 h and then rinsed with warm distilled water. Degummed silk (SF) was dissolved in a ternary solvent system of $CaCl_2/CH_3CH_2OH/H_2O$ (1:2:8 in molar ratio) at 70 ° C for 6 h. After dialysis with cellulose tubular membrane (Bialysis Tubing D9527 Sigma) in H_2O for 3 days, the SF solution was filtered and lyophilized to obtain the regenerated SF sponges.

Preparation of the spinning solution

SF solutions were prepared by dissolving the regenerated SF sponges in 98% formic acid for 30 min. Concentrations of SF solutions for electrospinning was in the range from 8% to 14% by weight.

Electrospinning

In the electrospinning process, a high electric potential (Gamma High voltage) was applied to a droplet of SF solution at the tip (0.35 mm inner diameter) of a syringe needle, The electrospun nanofibers were collected on a target plate which was placed at a distance of 10 cm from the syringe tip. The syringe tip and the target plate were enclosed in a chamber for adjusting and controlling the temperature. Schematic diagram of the electrospinning apparatus is shown in figure 1. The processing temperature was adjusted at 25, 50 and 75°C. A high voltage in the range from 10 kV to 20 kV was applied to the droplet of SF solution.

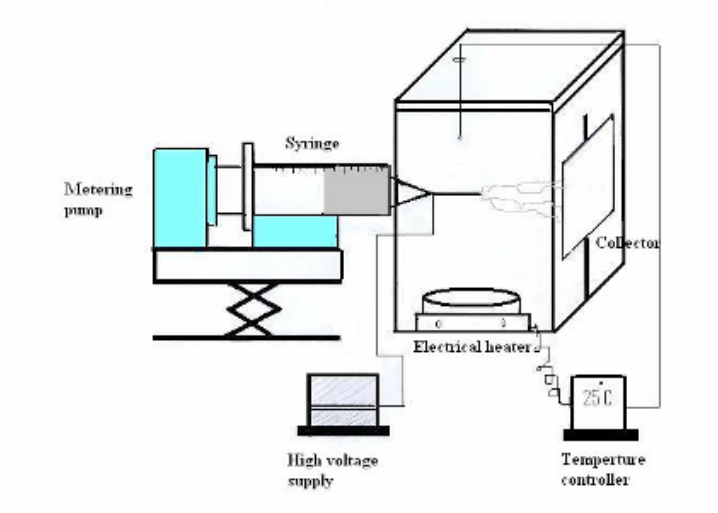

Fig1. Schematic diagram of electrospinning apparatus

Characterization

Optical microscope (Nikon Microphot-FXA) was used to investigate the macroscopic morphology of electrospun SF fibers. For better resolving power, morphology, surface texture and dimensions of the gold-sputtered electrospun nanofibers were determined using a Philips XL-30 scanning electron microscope. A measurement of about 100 random fibers was used to determine average fiber diameter and their distribution.

Results and discussions

Effect of silk concentration

One of the most important quantities related to electrospun nanofibers is their diameter. Since nanofibers are resulted from evaporation of polymer jets, the fiber diameters will depend on the jet sizes and the solution concentration. It has been reported that during the traveling of a polymer jet from the syringe tip to the collector, the primary jet may be split into different sizes multiple jets, resulting in different fiber diameters. When no splitting is involved in electrospinning, one of the most important parameters influencing the fiber diameter is concentration of regenerated silk solution. The jet with a low concentration breaks into droplets readily and a mixture of fibers, bead fibers and droplets as a result of low viscosity is generated. These fibers have an irregular morphology with large variation in size, on the other hand jet with high concentration does not break up but travels to the grounded target and tends to facilitate the formation of fibers without beads and droplets. In this case, fibers became more uniform with regular morphology [4-10].

At first, a series of experiments were carried out when the silk concentration was varied from 8 to 14% at the 15KV constant electric field and 25°C constant temperature. Below the silk concentration of 8% as well as at low electric filed in the case of 8% solution, droplets were formed instead of fibers. Figure 2 shows morphology of the obtained fibers from 8% silk solution at 20 KV. The obtained fibers are not uniform. The average fiber diameter is 72 nm and a narrow distribution of fiber diameters is observed. It was found that continuous nanofibers were formed above silk concentration of 8% regardless of the applied electric field and electrospinning condition.

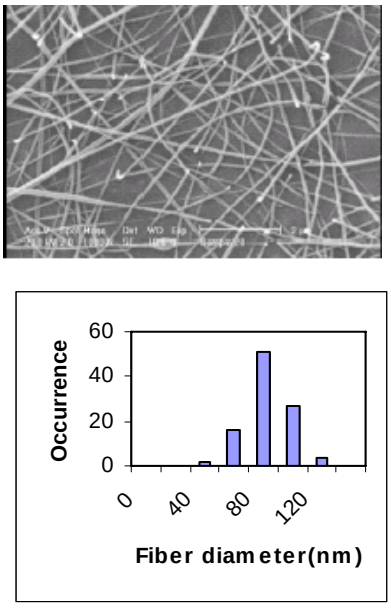

Fig.2. SEM micrograph and fiber distribution of 8wt% of silk at 20 KV and 25° C

In the electrospinning of silk fibroin, when the silk concentration is more than 10%, thin and rod like fibers with diameters range from 60-450 nm were obtained. Figures 3-5 show the SEM micrographs and diameter distribution of the resulted fibers.

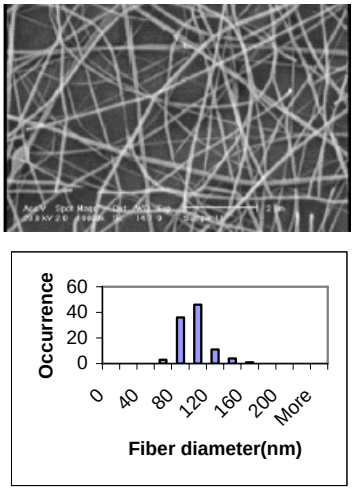

Fig.3.SEM micrograph and fiber distribution of 10wt% of silk at 15 KV and 25°C

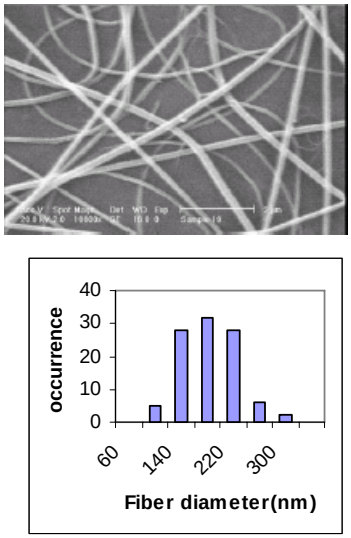

Fig.4.SEM micrograph and fiber distribution of 12wt% of silk at 15 KV and 25° C

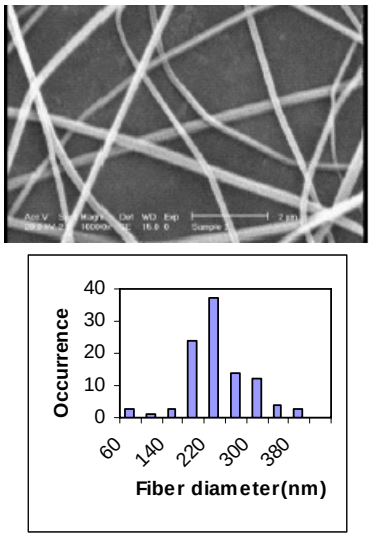

Fig.5.SEM micrograph and fiber distribution of 14wt% of silk at 15 KV and 25° C

There is a significant increase in mean fiber diameter with the increasing of the silk concentration, which shows the important role of silk concentration in fiber formation during electrospinning process. Concentration of the polymer solution reflects the number of entanglements of polymer chains in the solution, thus solution viscosity. Experimental observations in electrospinning confirm that for forming fibers, a minimum polymer concentration is required. Below this critical concentration, application of electric field to a polymer solution results electrospraying and formation of droplets to the instability of the ejected jet. As the polymer concentration increased, a mixture of beads and fibers is formed. Further increase in concentration results in formation of continuous fibers as reported in this paper. It seems that the critical concentration of the silk solution in formic acid for the formation of continuous silk fibers is 10%.

Experimental results in electrospinning showed that with increasing the temperature of electrospinning process, concentration of polymer solution has the same effect on fibers diameter at 25°C. Figures 6-8 show the SEM micrographs and diameter distribution of the fibers at 50 °C.

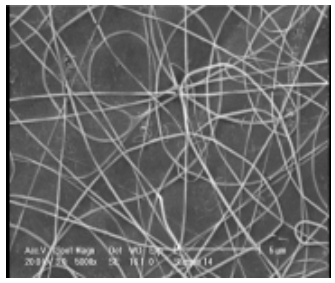

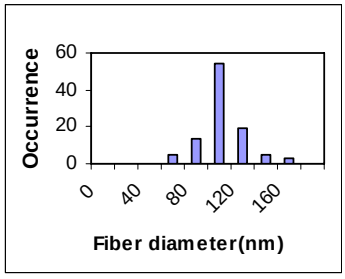

Fig.6.SEM micrograph and fiber distribution of 10wt% of silk at 15 KV and 50°C

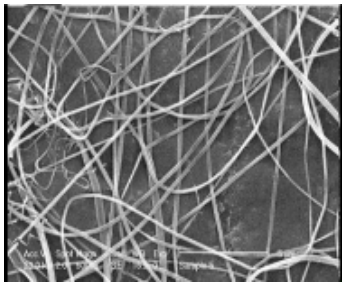

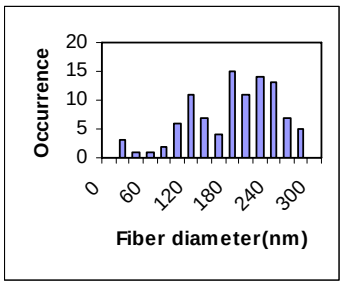

Fig.7.SEM micrograph and fiber distribution of 12wt% of silk at 15 KV and 50°C

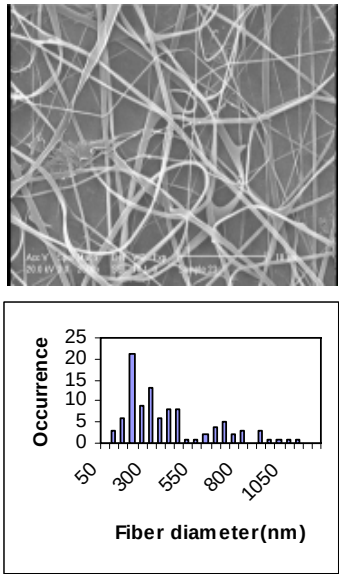

Fig.8.SEM micrograph and fiber distribution of 14wt% of silk at 15 KV and 50°C

When the temperature of the electrospinning process increased, the circular cross section became elliptical and then flat, forming a ribbon with a cross-sectional perimeter nearly the same as the perimeter of the jet. Flat and ribbon like fibers have greater diameter than circular fibers. It seems that at high voltage the primary jet splits into different sizes multiple jets, resulting in different fiber diameters that nearly in a same range of diameter.

At 75°C, the concentration and applied voltage have the same effect as 50°C. Figures 9-11 show the SEM micrographs and diameter distribution of nano fibers at 75°C.

Figure 12 shows the relationship between mean fiber diameter and SF concentration at different electrospinning temperature. There is a significant increase in mean fiber diameter with increasing of the silk concentration, which shows the important role of silk concentration in fiber formation during electrospinning process. It is well known that the viscosity of polymer solutions is proportional to concentration and polymer molecular weight. For concentrated polymer solution, concentration of the

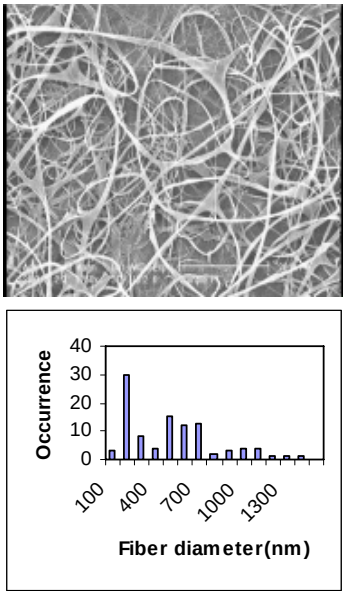

Fig.9.SEM micrograph and fiber distribution of 10wt% of silk at 15 KV and 75°C

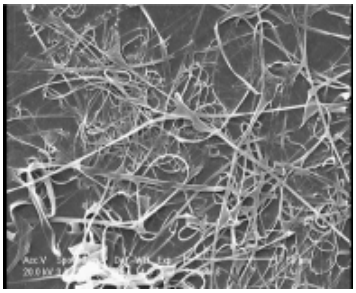

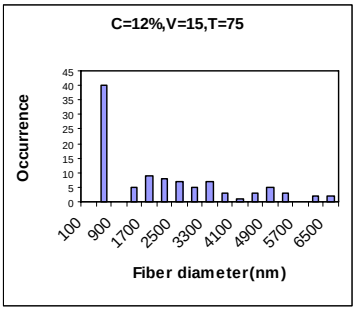

Fig.10.SEM micrograph and fiber distribution of 12wt% of silk at 15 KV and 75°C

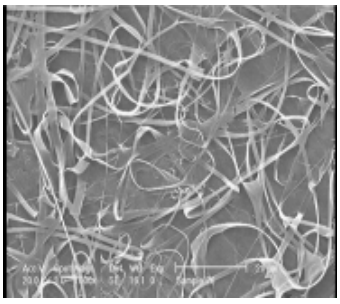

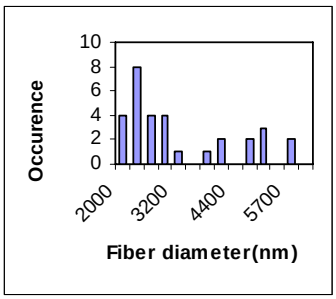

Fig.11.SEM micrograph and fiber distribution of 14wt% of silk at 15 KV and 75°C

polymer solution reflects the number of entanglements of polymer chains, thus have considerable effects on the solution viscosity. At fixed polymer molecular weight, the higher polymer concentration resulting higher solution viscosity. The jet from low viscosity liquids breaks up into droplets more readily and few fibers are formed, while at high viscosity, electrospinning is prohibited because of the instability flow causes by the high cohesiveness of the solution. Experimental observations in electrospinning confirm that for fiber formation to occur, a minimum polymer concentration is required. Below this critical concentration, application of electric field to a polymer solution results electro spraying and formation of droplets to the instability of the ejected jet. As the polymer concentration increased, a mixture of beads and fibers is formed. Further increase in concentration results in formation of continuous fibers as reported in this chapter. It seems that the critical concentration of the silk solution in formic acid for the formation of continuous silk fibers is 10% when the applied electric field was in the range of 10 to 20 kV.

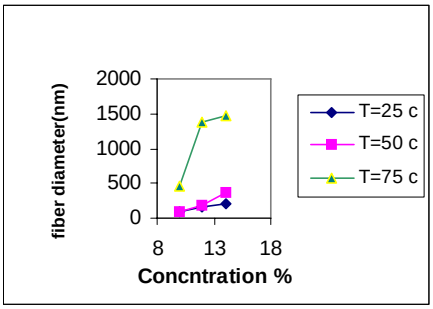

Fig.12. Mean fiber diameter of electrospun silk fibers at 25, 50 and 75°C at15 kV

Effect of electric field

It was already reported that the effect of the applied electrospinning voltage is much lower that effect of the solution concentration on the diameter of electrospun fibers. In order to study the effect of the electric field, silk solution with the concentration of 10, 12, and 14% were electrospun at 10, 15, and 20 KV at 25°C. The variation of the mean fiber diameter at different applied voltage for different concentration is shown in fig. 13. This figure and SEM micrographs show that at all electric fields continuous and uniform fibers with different fiber diameter are formed. At a high solution concentration, effect of applied voltage is nearly significant. It is suggested that, at this temperature, higher applied voltage causes multiple jets formation, which would provide decrease of fiber diameter.

As the results of this finding it seems that electric field shows different effects on the nanofibers morphology. This effect depends on the polymer solution concentration and electrospinning conditions.

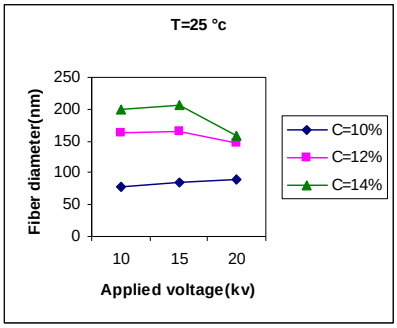

Fig.13.Mean fiber diameter of electrospun silk fibers at 10%, 15%, 20% and 25°C

Effect of electrospinning temperature

One of the most important quantities related with electrospun nanofibers is their diameter. Since nanofibers are resulted from evaporation of polymer jets, the fiber diameters will depend on the jet sizes**.** The elongation of the jet and the evaporation of the solvent both change the shape and the charge per unit area carried by the jet. After the skin is formed, the solvent inside the jet escapes and the atmospheric pressure tends to collapse the tube like jet. The circular cross section becomes elliptical and then flat, forming a ribbon-like structure. In this work we believe that ribbon-like structure in the electrospinning of SF at higher temperature thought to be related with skin formation at the jets. With increasing the electrospinning temperature, solvent evaporation rate increases, which results in the formation of skin at the jet surface. Non-uniform lateral stresses around the fiber due to the uneven evaporation of solvent and/or striking the target make the nanofibers with circular cross-section to collapse into ribbon shape.

Bending of the electrospun ribbons were observed on the SEM micrographs as a result of the electrically driven bending instability or forces that occurred when the ribbon was stopped on the collector. Another problem that may be occurring in the electrospinning of SF at high temperature is the branching of jets. With increasing the temperature of electrospinning process, the balance between the surface tension and electrical forces can shift so that the shape of a jet becomes unstable. Such an unstable jet can reduce its local charge per unit surface area by ejecting a smaller jet from the surface of the primary jet or by splitting apart into two smaller jets. Branched jets, resulting from the ejection of the smaller jet on the surface of the primary jet were observed in electrospun fibers of SF. The axes of the cones from which the secondary jets originated were at an angle near 90° with respect to the axis of the primary jet. Figure 14 shows the SEM micrographs of flat, ribbon like and branched fibers.

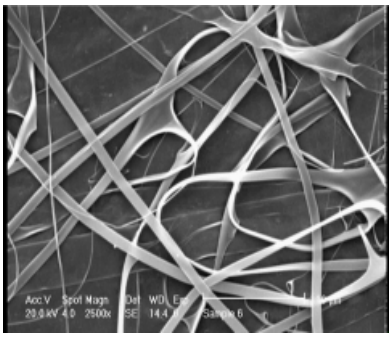

Fig.14. SEM micrograph of silk flat, ribbon like and branched nano fibers at high temperature

In order to study the effect of electrospinning temperature on the morphology and texture of electrospun silk nanofibers, 12% silk solution was electrospun at various temperatures of 25, 50 and 75°C. Results are shown in figure 15. Interestingly, the electrospinning of silk solution showed flat fiber morphology at 50 and 75°C, whereas circular structure was observed at 25°C. At 25°C, the nanofibers with a rounded cross section and a smooth surface were collected on the target. Their diameter showed a size range of approximately 100 to 300 nm with 180 nm being the most frequently occurring. They are within the same range of reported size for electrospun silk nanofibers. With increasing the electrospinning temperature to 50°C, the morphology of the fibers was slightly changed from circular cross section to ribbon like fibers. Fiber diameter was also increased to a range of approximately 20 to 320 nm with 180 nm the most occurring frequency. At 75°C, the morphology of the fibers was completely changed to ribbon like structure. Furthermore, fibers dimensions were increased significantly to the range of 500 to 4100 nm with 1100 nm the most occurring frequency.

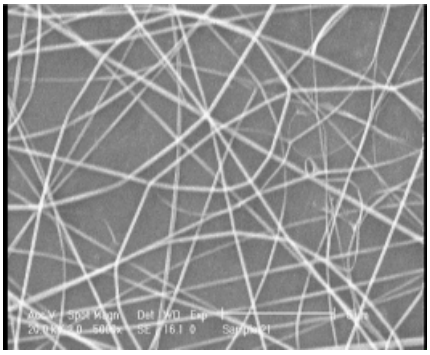

a

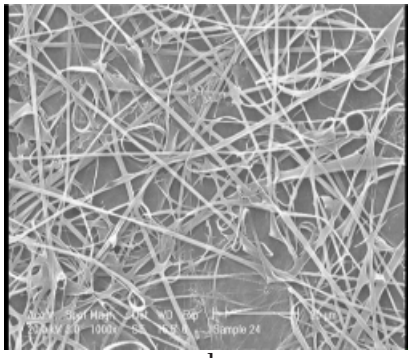

b

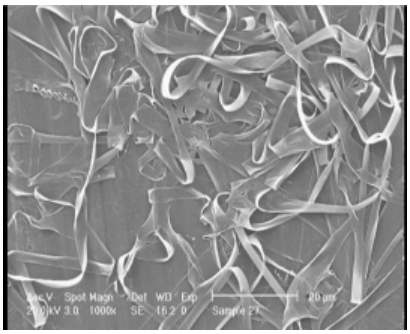

c

Fig.15. SEM micrograph of 12wt% of silk at 20 KV and (a) 25°C ,(b) 50 ° C, (c) 75°C

Experimental design

Response surface methodology (RSM) is a collection of mathematical and statistical techniques for empirical model building (Appendix). By careful design of *experiments*, the objective is to optimize a *response* (output variable) which is influenced by several *independent variables* (input variables). An experiment is a series of tests, called *runs*, in which changes are made in the input variables in order to identify the reasons for changes in the output response.

In order to optimize and predict the morphology and average fiber diameter of electrospun silk, design of experiment was employed in the present work. Morphology of fibers and distribution of fiber diameter of silk precursor were investigated varying concentration, temperature and applied voltage. A more systematic understanding of these process conditions was obtained and a quantitative basis for the relationships between average fiber diameter and electrospinning parameters was established using response surface methodology (Appendix), which will provide some basis for the preparation of silk nanofibers.

A central composite design was employed to fit a second-order model for three variables. Silk concentration (X_1), applied voltage (X_2), and temperature (X_3) were three independent variables (factors) considered in the preparation of silk nanofibers, while the fibers diameter were dependent variables (response). The actual and corresponding coded values of three factors (X_1, X_2, and X_3) are given in table 1. The following second-order model in X_1, X_2 and X_3 was fitted using the data in table 1.

$$Y = \beta_0 + \beta_1 x_1 + \beta_2 x_2 + \beta_3 x_3 + \beta_{11} x_1^2 + \beta_{22} x_2^2 + \\ + \beta_{33} x_3^2 + \beta_{12} x_1 x_2 + \beta_{13} x_1 x_3 + \beta_{23} x_2 x_3 + \varepsilon$$

The Minitab and Mathlab programs were used for analysis of this second-order model and for response surface plots (Minitab 11, Mathlab 7).

By regression analysis, values for coefficients for parameters and P-values (a measure of the statistical significance) are calculated. When P-value is less than 0.05, the factor has significant impact on the average fiber diameter. If P-value is greater than 0.05, the factor has no significant impact on average fiber diameter. R^2_{adj} (representing the proportion of the total variability that has been explained by the regression model) for regression models were obtained (table 2) and main effect plots on fiber diameter (fig 16) were obtained and reported.

The fitted second-order equation for average fiber diameter is given by:

$$Y = 391 + 311 X_1 - 164 X_2 + 57 X_3 - 162 X_1^2 + 69 X_2^2 + \\ + 391 X_3^2 - 159 X_1 X_2 + 315 X_1 X_3 - 144 X_2 X_3 \quad (1)$$

where Y = Average fiber diameter

		Coded values		
X_i	Independent variables	-1	0	1
X_1	Silk concentration (%)	10	12	14
X_2	applied voltage (KV)	10	15	20
X_3	temperature (° C)	25	50	75

Table 1
CENTRAL COMPOSITE DESIGN

Variables	Constant		P-value
	β_0	391.3	0.008
x_1	β_1	310.98	0.00
x_2	β_2	-164.0	0.015
x_3	β_3	57.03	0.00
x^2_1	β_{11}	161.8	0.143
x^2_2	β_{22}	68.8	0.516
x^2_3	β_{33}	390.9	0.002
x_1x_2	β_{12}	-158.77	0.048
x_1x_3	β_{13}	314.59	0.001
x_2x_3	β_{23}	-144.41	0.069
F	P-value	R^2	R^2 (adj)
18.84	0.00	0.907	0.858

Table 2
REGRESSION ANALYSIS FOR THE THREE FACTORS (CONCENTRATION, APPLIED VOLTAGE, TEMPERATURE) AND COEFFICIENTS OF THE MODEL IN CODED UNIT*

* Model: $Y=\beta o+\beta_1 x_{1+} \beta_2 x_{2+} \beta_3 x_3+ \beta_{11} x^2_1+ \beta_{22} x^2_2+ \beta_{332} x^2_3 + \beta_{12} x_1 x2_+ \beta_{13} x_1 x 3_+ \beta_{13} x_2 x3$ where "y" is average fiber diameter.

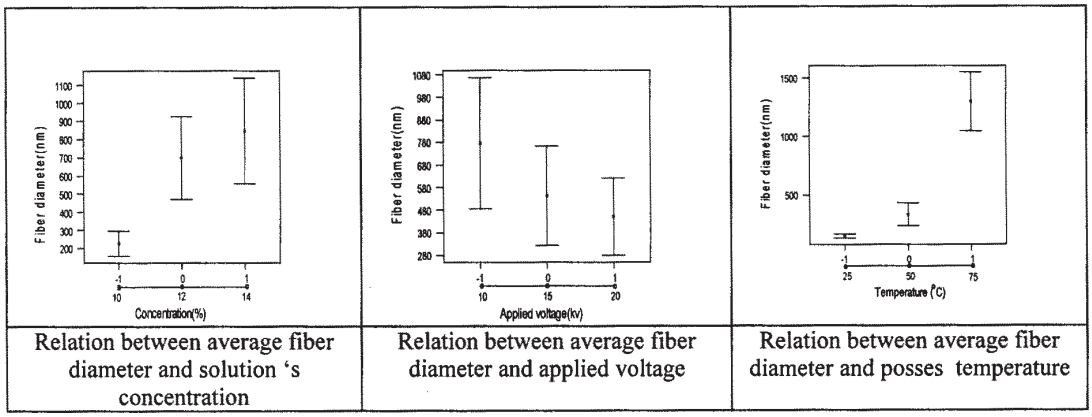

Relation between average fiber diameter and solution 's concentration | Relation between average fiber diameter and applied voltage | Relation between average fiber diameter and posses temperature

Fig.16. Effect of electrospinning parameters on silk nano fibers diameter

From the P-values listed in table 2, it is obvious that P-value of term X_2 is greater than P-values for terms X_1 and X_3. And other P-values for terms related to applied voltage such as, X_2^2, X_1X_2, X_2X_3 are much higher than significance level of 0.05. That is to say, applied voltage has no much significant impact on average fiber diameter and the interactions between concentration and applied voltage, temperature and applied voltage are not significant, either. But P-values for term related to X_3 and X_1 are less than 0.05. Therefore, temperature and concentration have significant impact on average fiber diameter. Furthermore, R^2_{adj} is 0.858, so this model explains 86% of the variability in new data.

Appendix

Variables which potentially can alter the electrospinning process (fig. A-1) are large. Hence, investigating all of them in the framework of one single research would almost be impossible. However, some of these parameters can be held constant during experimentation. For instance, performing the experiments in a controlled environmental condition, which is concerned in this study, the ambient parameters (i.e. temperature, air pressure, and humidity) are kept unchanged. Solution viscosity is affected by polymer molecular weight, solution concentration, and temperature. For a particular polymer (constant molecular weight) at a fixed temperature, solution concentration would be the only factor influencing the viscosity. In this circumstance, the effect of viscosity could be determined by the solution concentration. Therefore, there would be no need for viscosity to be considered as a separate parameter.

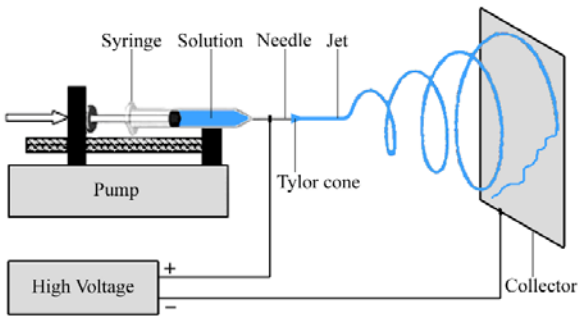

Fig. A-1: A typical image of Electrospinning process

In this regard, solution concentration (C), spinning distance (d), applied voltage (V), and volume flow rate (Q) were selected to be the most influential parameters. The next step is to choose the ranges over which these factors are varied. Process knowledge, which is a combination of practical experience and theoretical understanding, is required to fulfill this step. The aim is here to find an appropriate range for each parameter where dry, bead-free, stable, and continuous fibers without breaking up to droplets are obtained. This goal could be achieved by conducting a set of preliminary experiments while having the previous works in mind along with utilizing the reported relationships.

The relationship between intrinsic viscosity ([h]) and molecular weight (M) is given by the well-known Mark-Houwink-Sakurada equation as follows:

$$[\eta] = KM^a \qquad \text{(A-1)}$$

where K and a are constants for a particular polymer-solvent pair at a given temperature. Polymer chain entanglements in a solution can be expressed in terms of Berry number (B), which is a dimensionless parameter and defined as the product of intrinsic viscosity and polymer concentration ($B=[\eta]C$). For each molecular weight, there is a lower critical concentration at which the polymer solution cannot be electrospun.

As for determining the appropriate range of applied voltage, referring to previous works, it was observed that the changes of voltage lay between 5 kV to 25 kV depending on experimental conditions; voltages above 25 kV were rarely used. Afterwards, a series of experiments were carried out to obtain the desired voltage domain. At $V<10$ kV, the voltage was too low to spin fibers and 10 kV $\leq V<15$ kV resulted in formation of fibers and droplets; in addition, electrospinning was impeded at high concentrations. In this regard, 15 kV $\leq V \leq$ 5 kV was selected to be the desired domain for applied voltage.

The use of 5 cm – 20 cm for spinning distance was reported in the literature. Short distances are suitable for highly evaporative solvents whereas it results in wet coagulated fibers for nonvolatile solvents due to insufficient evaporation time. Afterwards, this was proved by experimental observations and 10 cm$\leq d \leq$ 20 cm was considered as the effective range for spinning distance.

Few researchers have addressed the effect of volume flow rate. Therefore in this case, the attention was focused on experimental observations. At $Q<0.2$ mL/h, in most cases especially at high polymer concentrations, the fiber formation was hindered due to insufficient supply of solution to the tip of the syringe needle. Whereas, excessive feed of solution at $Q>0.4$ mL/h incurred formation of droplets along with fibers. As a result, 0.2 mL/h $\leq Q \leq$ 0.4 ml/h was chosen as the favorable range of flow rate in this study.

Consider a process in which several factors affect a response of the system. In this case, a conventional strategy of experimentation, which is extensively used in practice, is the *one-factor-at-a-time* approach. The major disadvantage of this approach is its failure to consider any possible interaction between the factors, say the failure of one factor to produce the same effect on the response at different levels of another factor. For instance, suppose that

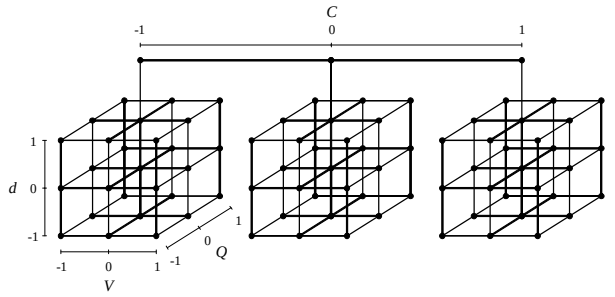

Fig. A-2: 3^4 full factorial experimental design used in this study

two factors A and B affect a response. At one level of A, increasing B causes the response to increase, while at the other level of A, the effect of B totally reverses and the response decreases with increasing B. As interactions exist between electrospinning parameters, this approach may not be an appropriate choice for the case of the present work. The correct strategy to deal with several factors is to use a full factorial design. In this method, factors are all varied together; therefore all possible combinations of the levels of the factors are investigated. This approach is very efficient, makes the most use of the experimental data and takes into account the interactions between factors.

It is trivial that in order to draw a line at least two points and for a quadratic curve at least three points are required. Hence, three levels were selected for each parameter in this study so that it would be possible to use quadratic models. These levels were chosen equally spaced. A full factorial experimental design with four factors (solution concentration, spinning distance, applied voltage, and flow rate) each at three levels (3^4 design) were employed resulting in 81 treatment combinations. This design is shown in figure A-2.

-1, 0, and 1 are coded variables corresponding to low, intermediate and high levels of each factor respectively. The coded variables (x_j) were calculated using Equation (A-2) from natural variables (ζ). The indices 1 to 4 represent solution concentration, spinning distance, applied voltage, and flow rate respectively. In addition to experimental data, 15 treatments inside the design space were selected as test data and used for evaluation of the models. The natural and coded variables for experimental data (numbers 1-81) as well as test data (numbers 82-96) are listed in **Error! Reference source not found.** in Appendix.

$$x_j = \frac{\xi_j - [\xi_{hj} + \xi_{lj}]/2}{[\xi_{hj} - \xi_{lj}]/2} \tag{A-2}$$

The mechanism of some scientific phenomena has been well understood and models depicting the physical behaviour of the system have been drawn in the form of mathematical relationships. However, there are numerous processes at the moment which have not been sufficiently understood to permit the theoretical approach. Response surface methodology (RSM) is a combination of mathematical and statistical techniques useful for empirical modeling and analysis of such systems. The application of RSM is in situations where several input variables are potentially influence some performance measure or quality characteristic of the process – often called responses. The relationship between the response (y) and k input variables ($\zeta_1,\zeta_2,...,\zeta_k$) could be expressed in terms of mathematical notations as follows:

$$y = f(\xi_1,\xi_2,...,\xi_k) \tag{A-3}$$

where the true response function f is unknown. It is often convenient to use coded variables ($x_1,x_2,..,x_k$) instead of natural (input) variables. The response function will then be:

$$y = f(x_1,x_2,...,x_k) \tag{A-4}$$

Since the form of true response function f is unknown, it must be approximated. Therefore, the successful use of RSM is critically dependent upon the choice of appropriate function to approximate f. Low-order polynomials are widely used as approximating functions. First order (linear) models are unable to capture the interaction between parameters which is a form of curvature in the true response function. Second order (quadratic) models will be likely to perform well in these circumstances. In general, the quadratic model is in the form of:

$$y = \beta_0 + \sum_{j=1}^{k}\beta_j x_j + \sum_{j=1}^{k}\beta_{jj}x_j^2 + \sum_{i<j}\sum_{j=2}^{k}\beta_{ij}x_i x_j + \varepsilon \tag{A-5}$$

where ε is the error term in the model. The use of polynomials of higher order is also possible but infrequent. The βs are a set of unknown coefficients needed to be estimated. In order to do that, the first step is to make some observations on the system being studied. The model in equation (A-5) may now be written in matrix notations as:

$$\mathbf{y} = \mathbf{X\beta} + \boldsymbol{\varepsilon} \tag{A-6}$$

where $\mathbf{y}$ is the vector of observations, $\mathbf{X}$ is the matrix of levels of the variables, $\boldsymbol{\beta}$ is the vector of unknown coefficients, and $\boldsymbol{\varepsilon}$ is the vector of random errors. Afterwards, method of least squares, which minimizes the sum of squares of errors, is employed to find the estimators of the coefficients ($\boldsymbol{\beta}$) through:

$$\hat{\boldsymbol{\beta}} = (\mathbf{X}'\mathbf{X})^{-1}\mathbf{X}'\mathbf{y} \tag{A-7}$$

The fitted model will then be written as:

$$\hat{\mathbf{y}} = \mathbf{X}\hat{\boldsymbol{\beta}} \tag{A-8}$$

Finally, response surfaces or contour plots are depicted to help visualize the relationship between the response and the variables and see the influence of the parameters. As you might notice, there is a close connection between RSM and linear regression analysis.

After the unknown coefficients (βs) were estimated by least squares method, the quadratic models for the mean fiber diameter (MFD) and standard deviation of fiber diameter (StdFD) in terms of coded variables are written as:

$$MFD = 282.031 + 34.953x_1 + 5.622x_2 - 2.113x_3 + 9.013x_4 - 11.613x_1^2 - 4.304x_2^2 - 15.500x_3^2 - 0.414x_4^2 + 12.517x_1x_2 + 4.020x_1x_3 - 0.162x_1x_4 + 20.643x_2x_3 + 0.741x_2x_4 + 0.877x_3x_4 \quad (A\text{-}9)$$

$$StdFD = 36.1574 + 4.5788x_1 - 1.5536x_2 + 6.4012x_3 + 1.1531x_4 - 2.2937x_1^2 - 0.1115x_2^2 - 1.1891x_3^2 + 3.0980x_4^2 - 0.2088x_1x_2 + 1.0010x_1x_3 + 2.7978x_1x_4 + 0.1649x_2x_3 - 2.4876x_2x_4 + 1.5182x_3x_4 \quad (A\text{-}10)$$

	F	p-value	R^2	R^2_{adj}	R^2_{pred}
MFD	106.02	0.000	95.74%	94.84%	93.48%
StdFD	42.05	0.000	89.92%	87.78%	84.83%

Table A-1
SUMMARY OF THE RESULTS FROM STATISTICAL ANALYSIS OF THE MODELS

In the next step, a couple of very important hypothesis-testing procedures were carried out to measure the usefulness of the models presented here. First, the test for significance of the model was performed to determine whether there is a subset of variables which contributes significantly in representing the response variations. The appropriate hypotheses are:

$$H_0 : \beta_1 = \beta_2 = \cdots = \beta_k$$
$$H_1 : \beta_j \neq 0 \quad \text{for at least one } j \quad (A\text{-}11)$$

The F statistics (the result of dividing the factor mean square by the error mean square) of this test along with the p-values (a measure of statistical significance, the smallest level of significance for which the null hypothesis is rejected) for both models are shown in table A-1.

The p-values of the models are very small (almost zero), therefore it could be concluded that the null hypothesis is rejected in both cases suggesting that there are some significant terms in each model. There are also included in table A-1, the values of R^2, R^2_{adj}, and R^2_{pred}. R^2 is a measure for the amount of response variation which is explained by variables and will always increase when a new term is added to the model regardless of whether the inclusion of the additional term is statistically significant or not. R^2_{adj} is the adjusted form of R^2 for the number of terms in the model; therefore it will increase only if the new terms improve the model and decreases if unnecessary terms are added. R^2_{pred} implies how well the model predicts the response for new observations, whereas R^2 and R^2_{adj} indicate how well the model fits the experimental data. The R^2 values demonstrate that 95.74% of MFD and 89.92% of StdFD are explained by the variables. The R^2_{adj} values are 94.84% and 87.78% for MFD and StdFD respectively, which account for the number of terms in the models. Both R^2 and R^2_{adj} values indicate that the models fit the data very well. The slight difference between the values of R^2 and R^2_{adj} suggests that there might be some insignificant terms in the models. Since the R^2_{pred} values are so close to the values of R^2 and R^2_{adj}, models do not appear to be overfit and have very good predictive ability.

The second testing hypothesis is evaluation of individual coefficients, which would be useful for determination of variables in the models. The hypotheses for testing of the significance of any individual coefficient are:

$$H_0 : \beta_j = 0$$
$$H_1 : \beta_j = 0 \quad (A\text{-}12)$$

The model might be more efficient with inclusion or perhaps exclusion of one or more variables. Therefore the value of each term in the model is evaluated using this test, and then eliminating the statistically insignificant terms, more efficient models could be obtained. The results of this test for the models of MFD and StdFD are summarized in table A-2 and table A-3 respectively. T statistic in these tables is a measure of the difference between an observed statistic and its hypothesized population value in units of standard error.

Table A-2
TEST ON INDIVIDUAL COEFFICIENTS FOR THE MODEL OF MEAN FIBER DIAMETER (MFD)

Term (coded)	Coeff.	T	p-value
Constant	282.031	102.565	0.000
C	34.953	31.136	0.000
d	5.622	5.008	0.000
V	-2.113	-1.882	0.064
Q	9.013	8.028	0.000
C^2	-11.613	-5.973	0.000
d^2	-4.304	-2.214	0.030
V^2	-15.500	-7.972	0.000
Q^2	-0.414	-0.213	0.832
Cd	12.517	9.104	0.000
CV	4.020	2.924	0.005
CQ	-0.162	-0.118	0.906
dV	20.643	15.015	0.000
dQ	0.741	0.539	0.592
VQ	0.877	0.638	0.526

Table A-3
TEST ON INDIVIDUAL COEFFICIENTS FOR THE MODEL OF STANDARD DEVIATION OF FIBER DIAMETER (STDFD)

Term (coded)	Coef	T	p-value
Constant	36.1574	39.381	0.000
C	4.5788	12.216	0.000
D	-1.5536	-4.145	0.000
V	6.4012	17.078	0.000
Q	1.1531	3.076	0.003
C^2	-2.2937	-3.533	0.001
d^2	-0.1115	-0.172	0.864
V^2	-1.1891	-1.832	0.072
Q^2	3.0980	4.772	0.000
Cd	-0.2088	-0.455	0.651
CV	1.0010	2.180	0.033
CQ	2.7978	6.095	0.000
dV	0.1649	0.359	0.721
dQ	-2.4876	-5.419	0.000
VQ	1.5182	3.307	0.002

As depicted, the terms related to Q^2, CQ, dQ, and VQ in the model of MFD and related to d^2, Cd, and dV in the model of StdFD have very high p-values, therefore they do not contribute significantly in representing the variation of the corresponding response. Eliminating these terms will enhance the efficiency of the models. The new models are then given by recalculating the unknown coefficients in terms of coded variables in equations (A-13) and (A-14),

and in terms of natural (uncoded) variables in equations (A-15), (A-16).

$$MFD = 281.755 + 34.953x_1 + 5.622x_2 - 2.113x_3 + 9.013x_4 - 11.613x_1^2 - 4.304x_2^2 - 15.500x_3^2 + 12.517x_1x_2 + 4.020x_1x_3 + 20.643x_2x_3 \quad \text{(A-13)}$$

$$StdFD = 36.083 + 4.579x_1 - 1.554x_2 + 6.401x_3 + 1.153x_4 - 2.294x_1^2 - 1.189x_3^2 + 3.098x_4^2 + 1.001x_1x_3 + 2.798x_1x_4 - 2.488x_2x_4 + 1.518x_3x_4 \quad \text{(A-14)}$$

$$MFD = 10.3345 + 48.7288C - 22.7420d + 7.9713V + 90.1250Q - 2.9033C^2 - 0.1722d^2 - 0.6120V^2 + 1.2517Cd + 0.4020CV + 0.8257dV \quad \text{(A-15)}$$

$$StdFD = -1.8823 + 7.5590C + 1.1818d + 1.2709V - 300.3410Q - 0.5734C^2 - 0.0476V^2 + 309.7999Q^2 + 0.1001CV + 13.9892CQ - 4.9752dQ + 3.0364VQ \quad \text{(A-16)}$$

The results of the test for significance as well as R^2, R^2_{adj}, and R^2_{pred} for the new models are given in table A-4. It is obvious that the *p*-values for the new models are close to zero indicating the existence of some significant terms in each model. Comparing the results of this table with Table A-1, the *F* statistic increased for the new models, indicating the improvement of the models after eliminating the insignificant terms. Despite the slight decrease in R^2, the values of R^2_{adj}, and R^2_{pred} increased substantially for the new models. As it was mentioned earlier in the paper, R^2 will always increase with the number of terms in the model. Therefore, the smaller R^2 values were expected for the new models, due to the fewer terms. However, this does not necessarily suggest that the pervious models were more efficient. Looking at the tables, R^2_{adj}, which provides a more useful tool for comparing the explanatory power of models with different number of terms, increased after eliminating the unnecessary variables. Hence, the new models have the ability to better explain the experimental data. Due to higher R^2_{pred}, the new models also have higher prediction ability. In other words, eliminating the insignificant terms results in simpler models which do not only present the experimental data in superior form, but also are more powerful in predicting new conditions.

The test for individual coefficients was performed again for the new models. The results of this test are summarized in table A-5 and table A-6. This time, as it was anticipated, no terms had higher *p*-value than expected, which need to be eliminated. Here is another advantage of removing unimportant terms. The values of *T* statistic increased for the terms already in the models implying that their effects on the response became stronger.

After developing the relationship between parameters, the test data were used to investigate the prediction ability of the models. Root mean square errors (RMSE) between the calculated responses (C_i) and real responses (R_i) were determined using equation (A-17) for experimental data as well as test data for the sake of evaluation of both MFD and StdFD models.

$$RMSE = \sqrt{\frac{\sum_{i=1}^{n}(C_i - R_i)^2}{n}} \quad \text{(A-17)}$$

Table A-4
SUMMARY OF THE RESULTS FROM STATISTICAL ANALYSIS OF THE MODELS AFTER ELIMINATING THE INSIGNIFICANT TERMS

	F	*p*-value	R^2	R^2_{adj}	R^2_{pred}
MFD	155.56	0.000	95.69%	95.08%	94.18%
StdFD	55.61	0.000	89.86%	88.25%	86.02%

Table A-5
TEST ON INDIVIDUAL COEFFICIENTS FOR THE MODEL OF MEAN FIBER DIAMETER (MFD) AFTER ELIMINATING THE INSIGNIFICANT TERMS

Term (coded)	Coeff.	*T*	*p*-value
Constant	281.755	118.973	0.000
C	34.953	31.884	0.000
d	5.622	5.128	0.000
V	-2.113	-1.927	0.058
Q	9.013	8.221	0.000
C^2	-11.613	-6.116	0.000
d^2	-4.304	-2.267	0.026
V^2	-15.500	-8.163	0.000
Cd	12.517	9.323	0.000
CV	4.020	2.994	0.004
dV	20.643	15.375	0.000

Table A-6
TEST ON INDIVIDUAL COEFFICIENTS FOR THE MODEL OF STANDARD DEVIATION OF FIBER DIAMETER (StdFD) AFTER ELIMINATING THE INSIGNIFICANT TERMS

Term (coded)	Coef	*T*	*p*-value
Constant	36.083	45.438	0.000
C	4.579	12.456	0.000
d	-1.554	-4.226	0.000
V	6.401	17.413	0.000
Q	1.153	3.137	0.003
C^2	-2.294	-3.602	0.001
V^2	-1.189	-1.868	0.066
Q^2	3.098	4.866	0.000
CV	1.001	2.223	0.029
CQ	2.798	6.214	0.000
dQ	-2.488	-5.525	0.000
VQ	1.518	3.372	0.001

Conclusions

The electrospinning of silk fibroin was processed and the average fiber diameters depend on the electrospinning condition. Morphology of fibers and distribution of diameter were investigated at various concentrations, applied voltages and temperature. The electrospinning temperature and the solution concentration have a significant effect on the morphology of the electrospun silk nanofibers. There effects were explained to be due to the change in the rate of skin formation and the evaporation rate of solvents. To determine the exact mechanism of the conversion of polymer into nanofibers require further theoretical and experimental work.

From the practical view the results of the present work can be condensed. Concentration of regenerated silk solution was the most dominant parameter to produce

uniform and continuous fibers. The jet with a low concentration breaks into droplets readily and a mixture of fibers and droplets as a result of low viscosity is generated. On the other hand jets with high concentration do not break up but traveled to the target and tend to facilitate the formation of fibers without beads and droplets. In this case, fibers become more uniform with regular morphology. In the electrospinning of silk fibroin, when the silk concentration is more than 10%, thin and rod like fibers with diameters range from 60-450 nm were obtained. Furthermore, In the electrospinning of silk fibroin, when the process temperature is more than 25°C, flat, ribbon like and branched fibers with diameters range from 60-7000 nm were obtained.

Two- way analysis of variance was carried out at the significant level of 0.05 to study the impact of concentration, applied voltages and temperature on average fiber diameter. It was concluded that concentration of solution and electrospinning temperature were the most significant factors impacting the diameter of fibers. Applied voltage had no significant impact on average fiber diameter. The average fiber diameter increased with polymer concentration and electrospinning temperature according to proposed relationship under the experimental conditions studied in this chapter.

References

1. M. ZIABARI, V. MOTTAGHITALAB, A. K. HAGHI, Simulated image of electrospun nonwoven web of PVA and corresponding nanofiber diameter distribution, Korean Journal of Chemical engng , Vol.25, No. 4, p. 919-922 ,2008.

2. M. ZIABARI, V. MOTTAGHITALAB, A. K. HAGHI, Evaluation of electrospun nanofiber pore structure parameters, Korean Journal of Chemical engng Vol.25, No. 4, p. 923-932 ,2008.

3. M. ZIABARI, V. MOTTAGHITALAB, A. K. HAGHI, Distance transform algoritm for measuring nanofiber diameter, Korean Journal of Chemical engng, Vol25, No. 4, p. 905-918 ,2008.

4. D. LI, Y. XIA, Electrospinning of Nanofibers: Reinventing the Wheel?, Advanced Materials, vol. 16, no. 14, p. 1151-1170, 2004.

5. R. DERCH, A. GREINER, J.H. WENDORFF, Polymer Nanofibers Prepared by Electrospinning, In: J. A. Schwarz, C. I. Contescu and K. Putyera, Dekker Encyclopedia of Nanoscience and Nanotechnology, CRC, New York, 2004.

6. A.K. HAGHI, M. AKBARI, Trends in Electrospinning of Natural Nanofibers. Physica Status Solidi (a), vol. 204, pp. 1830-1834, 2007.

7. P.W. Gibson, H.L. Schreuder-Gibson and D. Rivin, Electrospun Fiber Mats: Transport Properties, AIChE Journal, vol. 45, no. 1, p. 190-195, 1999.

8. Z.M. HUANG, Y.Z. ZHANG, M. KOTAKI, S. RAMAKRISHNA, A Review on Polymer Nanofibers by Electrospinning and Their Applications in Nanocomposites, Composites Science and Technology, vol. 63, p. 2223-2253, 2003.

9. M. LI, M.J. MONDRINOS, M.R. GANDHI, F.K. KO, A.S. WEISS, P.I. LELKES, Electrospun Protein Fibers as Matrices for Tissue Engineering, Biomaterials, vol. 26, p. 5999-6008, 2005.

10.E.D. BOLAND, B.D. COLEMAN, C.P. BARNES, D.G. SIMPSON, G.E. WNEK, G.L. BOWLIN, Electrospinning Polydioxanone for Biomedical Applications, Acta Biomaterialia, vol. 1, p. 115-123, 2005

Manuscript received: 10.06.2012